Sheng *et al. PhotoniX* (2022) 3:4
https://doi.org/10.1186/s43074-022-00050-8

PhotoniX

RESEARCH Open Access

Intracavity spherical aberration for selective generation of single-transverse-mode Laguerre-Gaussian output with order up to 95

Quan Sheng[1,2], Aihua Wang[1,2], Yuanyuan Ma[3*], Sijia Wang[4], Meng Wang[1,2], Zheng Shi[1,2], Junjie Liu[1,2], Shijie Fu[1,2], Wei Shi[1,2*], Jianquan Yao[1,2] and Takashige Omatsu[3]

*Correspondence: mayuanyuan612@gmail.com; shiwei@tju.edu.cn
[1] School of Precision Instrument and Optoelectronics Engineering, Institute of Laser and Optoelectronics, Tianjin University, Tianjin 300072, China[3] Molecular Chirality Research Center, Chiba University, 1-33 Yayoi-cho, Inage-ku, Chiba 263-8522, Japan
Full list of author information is available at the end of the article

Abstract

We investigate the generation of single-transverse-mode Laguerre-Gaussian (LG) emission from a diode-end-pumped Nd:YVO_4, 1064 nm laser using mode selection via intracavity spherical aberration (SA). We present both theoretical and experimental investigations, examining the limits of the order (both radial and angular indices) of the LG modes which can be produced, along with the resultant output power. We found that in order to generate single-mode emission of low-order LG modes which have relatively small beam diameters, lenses with shorter focal-length were required (to better differentiate neighboring LG modes via SA). The converse was true of LG modes with high-order. Through appropriate choice of the focal length of the intracavity lens, we were able to generate single-mode, $LG_{0,\pm m}$ laser output with angular indices m selectable from 1 to 95, as well as those with non-zero radial indices p of up to 4.

Keywords: Laguerre-Gaussian mode, Optical vortex laser, Spherical aberration, High-order mode, Mode selection

Introduction

Generation of structured light fields have been one of the most active topics of laser physics research because of their diverse range of applications [1–5] and their interesting dynamics [6–9]. Direct-generation of structured light from light sources, for example, through selecting particular high-order transverse modes directly from a laser cavity, benefits superior power handling, beam quality and conversion efficiency compared with approaches based on external-cavity reshaping [1, 2]. The Laguerre-Gaussian (LG) modes are an important family of structured light, whose field distributions are described by Laguerre polynomials functions. LG modes are eigenmodes of a cavity with cylindrical coordinates, which means that they can be obtained directly from a laser cavity which incorporates an appropriate mode-selection technique [10]. Demonstrated approaches to direct-generation of high-order LG modes from laser cavities include ring-shaped pump beams, intracavity phase modulating elements, a cavity mirror with a defect spot and via natural or thermal birefringence [2, 11–21]. The mechanism by

which these approaches work is the introduction of mode-varying gain or loss to the different orders of LG modes within the laser cavity, ensuring that there is sufficient net-gain difference between the desired order of mode and its neighboring modes.

Spherical aberration (SA) is an inherent aberration of spherical optics. It results in varied focal positions when beams with different widths are incident on a spherical lens. Considering that the beam radii of the ring-like $LG_{p,m}$ modes vary with radial and angular indices, p and m, the optical paths of different orders of LG modes may therefore be differentiated by SA, making mode-selection possible. In 2009, Senatsky et al. demonstrated multimode circular output from an end-pumped Yb:YAG ceramic laser, with a short-focal lens in the cavity to introduce strong SA [22]. Later, the same group realized single high-order LG mode output by increasing the cavity length to 80 cm (and longer) in order to narrow the "operating zone" of certain modes [23–25]. In our recent work, we demonstrated that single high-order LG mode operation can be achieved with a more compact cavity arrangement, by enhancing the SA via the use of a second lens in the cavity [26]. In that work, the angular index m of the $LG_{0,\pm m}$ output ranged from 10 to 33, and was selectable by simply adjusting the distance between the lens and the output coupler within a small range of 0.5 mm. Such SA-based approaches allow the direct generation of proper higher-order LG modes with high quality as an eigen mode from the laser cavity even without any custom-designed elements, such as intracavity phase modulating devices and defect spot mirrors.

In this work, we further characterize the spherical aberration-induced cavity loss on LG mode selection. Since the LG mode itself has non-negligible ring width, strong SA will also introduce significant loss to high-order modes which are supposed to be well retro-reflected, hence preventing them from oscillating. We modeled the influence of beam size and ring width of LG modes on the SA and found that managing the SA by choosing appropriate lens focal length is extremely important for generating desired orders of LG modes. In the experiment, the highest angular index m of the $LG_{0,\pm m}$ mode output reached 95 using a long-focal-length lens which has low SA-induced loss. Using a short-focal lens to enhance the mode-selecting capability, the lower-order mode of $LG_{0,\pm 1}$ as well as LG modes output with non-zero radial indices p were obtained.

Methods

Relationship between SA and LG modes

In our prior work, single-transverse-mode $LG_{0,\pm m}$ laser emission could be produced with angular index m between 10 and 33 when using lenses L1 and L2 with focal lengths of 150 mm and 33.9 mm, respectively. The mechanism by which high-order $LG_{0,\pm m}$ modes can be selected via SA is depicted in Fig. 1 of ref [26]. The laser oscillates with multiple modes when the output coupler M2 is located at the focal point of the LG beams (with m below 10). This configuration has limited mode-selecting capability. In contrast, we can expect that single-transverse-mode oscillation of lower-order LG modes can be achieved by using lens L2 with a shorter focal length to enhance the effect of SA.

It was observed that the output power of the generated modes decreased as the value of m increased, with the laser ceasing oscillation for values of $d3$ less than that required for LG beams with m values beyond 33. One reason for this decrease in power and eventual cessation of lasing is a progressive deterioration of the overlap between the

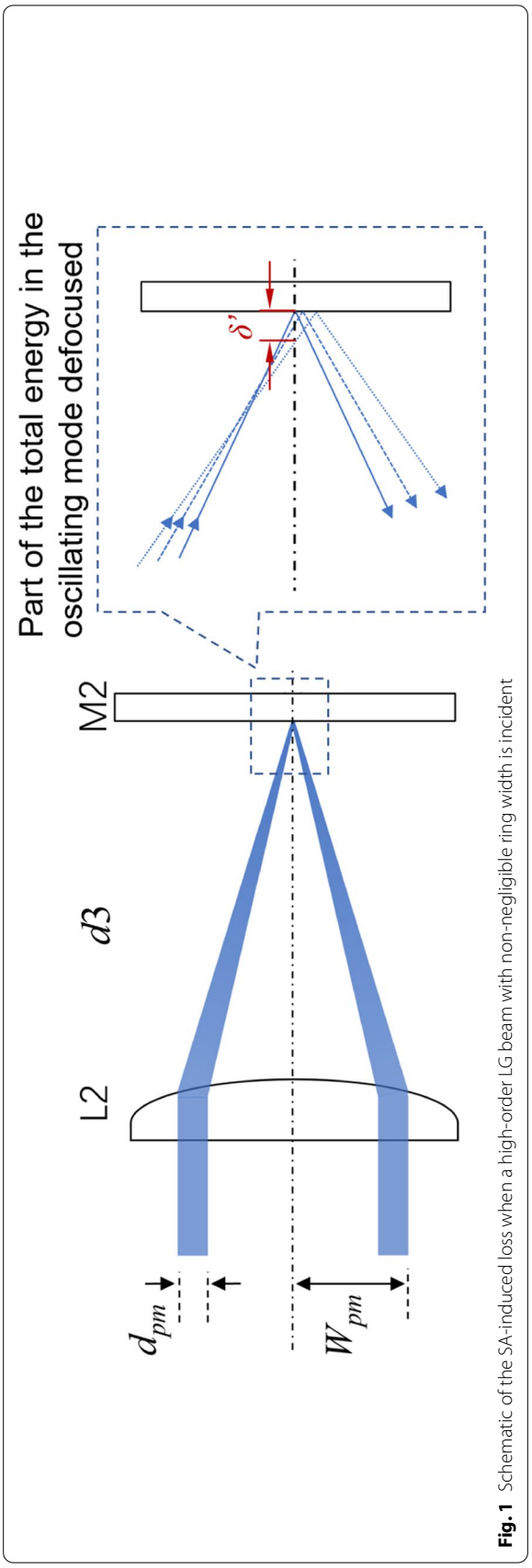

Fig. 1 Schematic of the SA-induced loss when a high-order LG beam with non-negligible ring width is incident

high-order LG mode (which has an ever-increasing hollow-core diameter) and the laser pump beam (which has a Gaussian intensity profile) within the laser crystal. Another contributing factor is the SA-induced loss on the oscillating modes. Fig. 1 depicts what happens when a ring-like LG mode with non-negligible ring width $d_{p,m}$ is focused by a lens L2 and reflected by a mirror M2 near the focal point. The cat-eye optics formed by L2 and M2 can only retro-reflect the beams which have focal points exactly on the mirror. As shown in Fig. 1, for a high-order LG mode with a finite ring width $d_{p,m}$, not all the rays achieve focus at the mirror due to the effect of SA. This means that not all of the energy in the ring-like beam is well retro-reflected, and parts of the beam suffers SA-induced loss [27]. It should be noted that the loss is much lower than those of other modes which are far more defocused and prohibited from oscillating. The amount of loss increases accordingly with stronger SA.

The size of a high-order LG mode is typically defined by its second-order intensity moment [28], which obeys Eq. 1 in [26]. However, since we plan to use the beam radius and ring width to describe how strongly the ring-shaped beam is defocused, it is important that the two parameters indicate where the energy is and how it is distributed. Therefore, we define the beam radius $W_{p,m}$ as the radius of the circle which contains 86.5% of the total energy of the beam, and the ring width $d_{p,m}$ as the difference between this radius and the radius of another circle which contains 13.5% of the total energy. The displacement of the focal point induced by the SA on a high-order LG beam with a beam radius $W_{p,m}$ and a ring width $d_{p,m}$ is δ' (in contrast to δ, which represents the displacement of the actual focal points from the nominal focal point of the lens) marked in Fig. 1, it is easy to see that larger δ' will result in higher loss for the oscillating mode.

Figure 2 shows the calculated the beam radius $W_{p,m}$ and the ring width $d_{p,m}$ of each $LG_{p,m}$ mode, which are normalized to the lowest order "fundamental" mode beam radius w, using the intensity distribution given by Eq. 2 in [28]. It can be seen

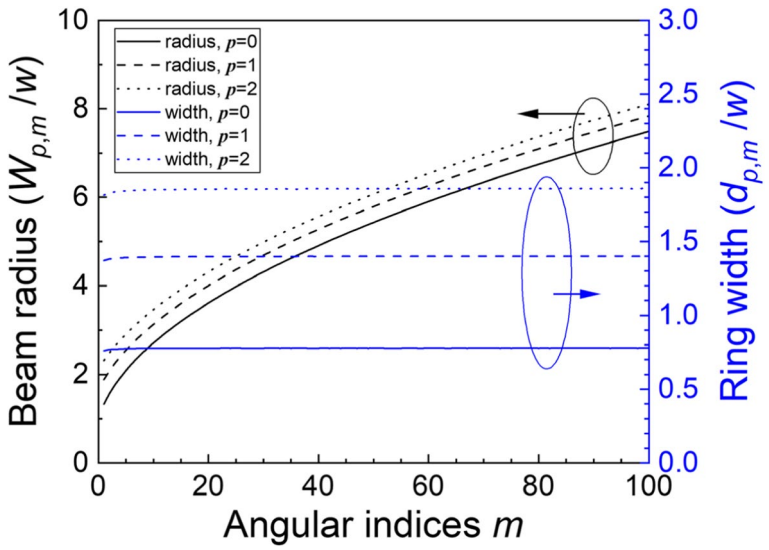

Fig. 2 The beam radius $W_{p,m}$ and ring width $d_{p,m}$ of LG modes normalized to the lowest order "fundamental" mode radius w, as a function of angular indices m, with radial indices p of 0, 1 and 2

that the beam radius $W_{p,m}$ (black lines) is an increasing function of p and m, while the ring width $d_{p,m}$ (blue lines) does not exhibit an obvious increase with the non-zero angular index m but increase dramatically with radial index p. Since the slope of the SA-induced focal point displacement increases with the beam size, a higher-order oscillating laser mode with a larger beam radius would suffer SA-induced loss which is higher than that of a lower-order oscillating mode with a smaller beam radius. This can be seen more clearly in Fig. 3, which shows the calculated displacement of the focal points of beams with certain width, from the nominal focal point of a $f = 33.9$ mm plano-convex N-BK7 lens. The ring width $d_{p,m}$ of the $LG_{0,30}$ and the $LG_{0,5}$ modes are marked on the curve, and these are based on the calculated fundamental mode beam radius w of 600 μm at the lenses L1 and L2 using ABCD matrices. The gray zone represents the $d_{p,m}$ between the two circles which contains 13.5% and 86.5% of the total energy. The intersections of the two boundaries of a gray zone and the SA curve indicate the SA-induced focal point displacement δ' and are indicative of the loss on the oscillating mode. For the $LG_{0,30}$ mode, the radii of the circles which contain 13.5% and 86.5% of total energy are 2.12 mm and 2.59 mm respectively. This results in a focal point displacement δ' of 0.30 mm across the ring with width $d_{p,m}$ of 0.47 mm. For the $LG_{0,5}$ mode with a much smaller beam size (with circle radii of 0.79 mm and 1.25 mm) but similar ring width, the focal point displacement δ' was reduced significantly to 0.12 mm. It is indicated that the displacement δ' increases with both the beam radius $W_{p,m}$ and the ring width $d_{p,m}$ from Fig. 3. For modes with higher-order angular indices m and resultant larger beam radius $W_{p,m}$, the SA-induced defocusing can be much more significant than that of the lower-order modes with similar ring width $d_{p,m}$ but smaller beam radius $W_{p,m}$. This is a contributing factor as to why the output power of higher-order modes are lower than those

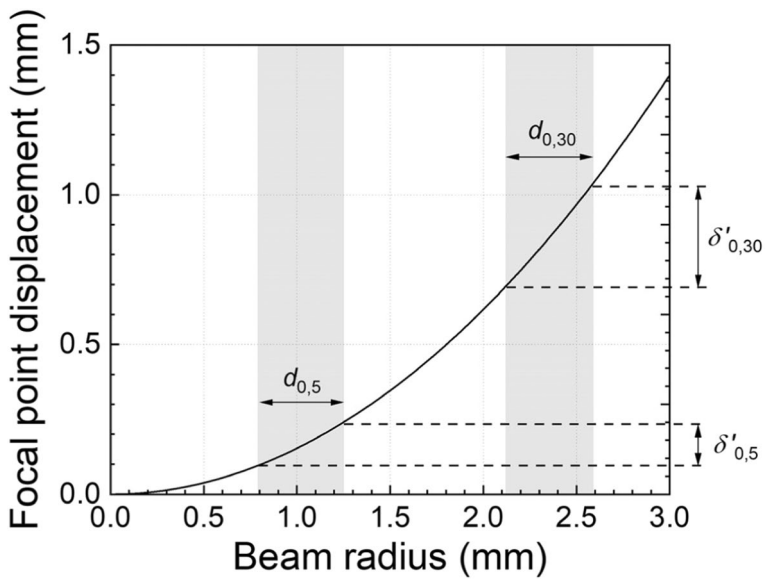

Fig. 3 The SA-induced focal point displacement (relative to the nominal focal position) as a function of beam radius at the lens L2. The gray zone shows the ring widths $d_{p,m}$ of certain modes. Their intersection with the SA curve is indicative of the effect that SA has on the beam (the calculated fundamental beam radius is 600 μm and the lens L2 is a plano-convex N-BK7 lens with $f = 33.9$ mm at 1064 nm)

of lower-order modes, and is a mechanism by which they can be suppressed. If the oscillation of higher-order modes is desired, one should therefore use a lens L2 with weaker SA to reduce the impact of SA-induced loss.

We also calculated the SA-induced focal-point displacement with different beam radius $W_{p,m}$ and ring width $d_{p,m}$, as shown in Fig. 4. A number of representative modes are marked. It reveals that higher-order modes with larger beam radius $W_{p,m}$ and ring width $d_{p,m}$ suffer larger δ' and higher resultant loss. This explains why the single, high-order mode output was obtained only with the radial index p of 0 in our previous work [26]. Single-mode operation can be achieved only when the SA is strong enough to differentiate neighboring modes. However, this comes with the caveat in that with the use of SA strong enough for single-transverse-mode operation, modes with nonzero radial index p (with corresponding much larger ring width $d_{p,m}$) will also suffer significant SA-induced loss and will be suppressed. It is therefore critical that lenses with the appropriate parameters (focal length, shape and substrate) and spacing $d3$ are chosen carefully in order to promote the generation of the desired order of LG laser mode.

It is worth mentioning that L2 with a shorter focal length than 33.9 mm provides almost the same SA-induced loss with non-zero p modes (LG modes with non-zero p) possessing small m. In fact, the focal displacement δ' of non-zero p modes with $m = 5$ is only within 0.12–0.35 mm, while this value for non-zero p modes with $m = 95$ is in the range of 0.5–1.3 mm, as plotted in Fig. 4. Also, the non-zero p modes possess typically a wider mode field than zero p modes, thereby yielding a better spatial overlap with a gain volume. Thus, the system will then allow the laser operation of non-zero p modes.

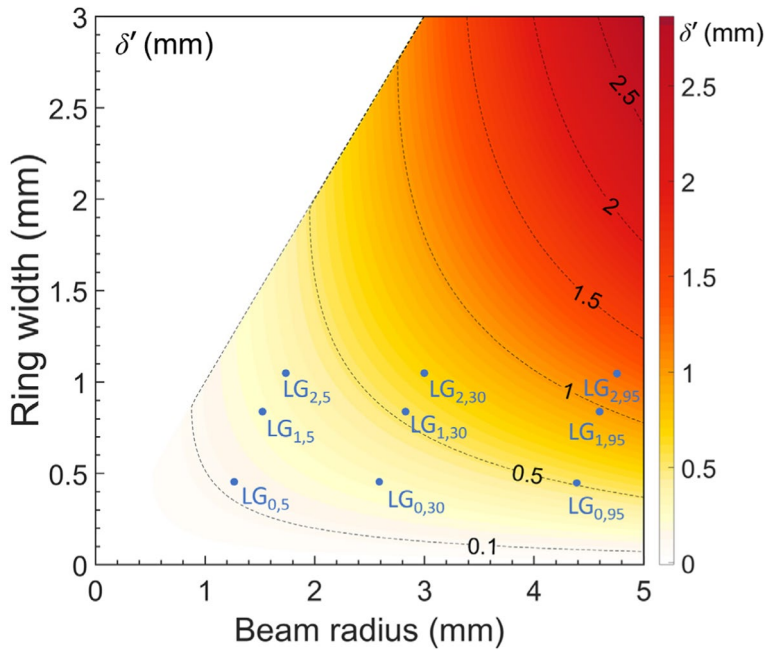

Fig. 4 Contour plot of the SA-induced focal point displacement δ' as a function of beam radius $W_{p,m}$ and ring width $d_{p,m}$ (with the $f = 33.9$ mm lens L2)

Experimental arrangement

The experimental setup of the scalar (linearly polarized) LG mode laser is depicted in Fig. 5. Similar to that in our prior work [26], the laser cavity was composed of a plano-concave total reflector M1 with a radius of curvature of 50 mm and a flat output coupler M2 with a transmittance of 10% at 1064 nm. The pump light from a 878.6 nm laser diode was focused with a beam radius of 120 μm into the laser crystal, an a-cut Nd:YVO_4 crystal with dimensions of $3 \times 3 \times 5$ mm^3 and doping concentration of 0.5-at.%. Two focusing lenses L1 and L2 were inserted in the cavity, to expand and collimate the intracavity beam and refocus it to induce SA for mode selection. L1 had a focal length of 150 mm and was located 155 mm ($d1$) from the crystal, while the distance $d3$ from L2 to M2 was the manufacturer-specified focal length of L2. As discussed in the previous section, the flat output coupler M2 will only provide feedback for the cavity mode whose focal point is on it, and hence the selective oscillation of different orders of LG modes can be achieved through adjusting the distance $d3$. This was done by mounting M2 onto a micrometer-driven translation stage. The laser output from M2 was then collimated by a lens L3 and refocused by another lens L4, to record the near- and far-field beam patterns using a CCD camera (Ophir SP907).

Results and discussions

Based on the analysis in Sect. 2, here, we used lenses L2 with different focal lengths, to extend the range of single LG mode outputs which could be generated. All the lenses used were of a N-BK7 substrate and were coated anti-reflecting at 1064 nm. For higher-order mode output, a bi-convex lens with 51.8 mm focal length and resultant weaker SA was used instead of the $f = 33.9$ mm plano-convex lens used in our prior work. In comparison to our prior work, when using the same incident diode pump power of 1.03 W, it was observed that the near-field beam pattern in this work became hollow when the output coupler M2 was moved towards the lens L2 by ~ 3 mm, from the position where the lowest-order, Gaussian "fundamental" mode was generated (defined as $\delta = 0$). However, the hollow beam was found to be propagation-variant, meaning that the output from the laser was comprised of multiple-transverse-modes. This characteristic was observed for values of δ from 3 mm to 4.42 mm. A propagation-invariant single-transverse-mode output of $LG_{0,\pm 27}$ was obtained when δ reached 4.42 mm, and this beam had a power of 127 mW. The lowest-order, single-transverse-mode output that could be obtained from the cavity had an angular index m of 27, which was higher than the $m = 10$ obtained with the $f = 33.9$ mm lens used in our prior work. This is because the $f = 51.8$ mm lens did not provide sufficient SA to distinguish the lower-order modes with smaller beam sizes. By decreasing the distance $d3$, higher-order mode outputs with lower power were obtained. Just prior to cessation of laser operation (for this fixed pump power), an output with a maximum angular index m of 75 and 11 mW output power was observed (with a value, δ of 5.14 mm). As expected, lower SA corresponds to lower loss, thus allowing higher-order modes with larger beam size to oscillate under the same pump power, even with worse overlap with the pump beam.

Increasing the incident pump power is a straight-forward method to overcome the large loss impacting the higher-order modes. Therefore, we increased the pump power

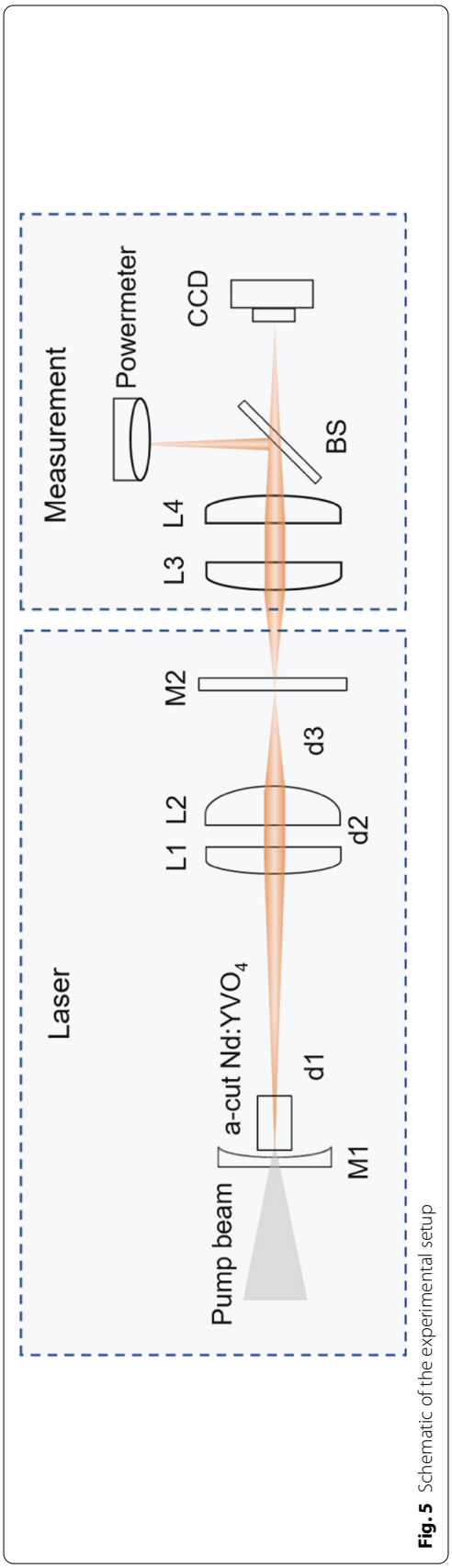

Fig. 5 Schematic of the experimental setup

a little from 1.03 W to 1.20 W. In doing so, single $LG_{0,\pm m}$ mode output with m ranging from 32 to 95 could be generated, with δ changing from 4.5 mm to 5.6 mm (correspondingly the distance $d3$ decreased by 1.1 mm). Such high-order LG mode laser is beneficial to be applied in cutting-edge fields such as space-divison multiplexing/demultiplexing optical/quantum communication and optical tapping/manipulation with the OAM freedom [3, 29, 30]. The laser output power decreased from 132 to 2 mW during this process. Fig. 6 shows some typical beam patterns recorded using the CCD camera, using the $f = 51.8$ mm lens (L2) and an incident pump power of 1.20 W. The intensity pattern is petal-like due to the coherent superposition of $LG_{0,+m}$ and $LG_{0,-m}$ modes. The angular indices m are determined by counting the dark bars around the circumference of the pattern.

We investigated the generation of single-transverse-mode output of lower-order LG modes via the application of lenses with shorter focal lengths (to induce strong SA). When using a plano-convex lens (L2) with a focal length of 25.4 mm, lower-order LG modes could be generated with angular indices m ranging from 2 to 16 and with non-zero radial indices p of up to 4. Shown in Fig. 7 are some typical patterns obtained using the $f = 25.4$ mm lens. It is clear that the generated LG modes are asymmetric. This is due to breaking of the cylindrical symmetry of the laser cavity, an effect which may be caused by misaligned optical elements or thermal lensing inside the cavity. Such asymmetric LG modes can be described as Ince-Gaussian modes (i.e.

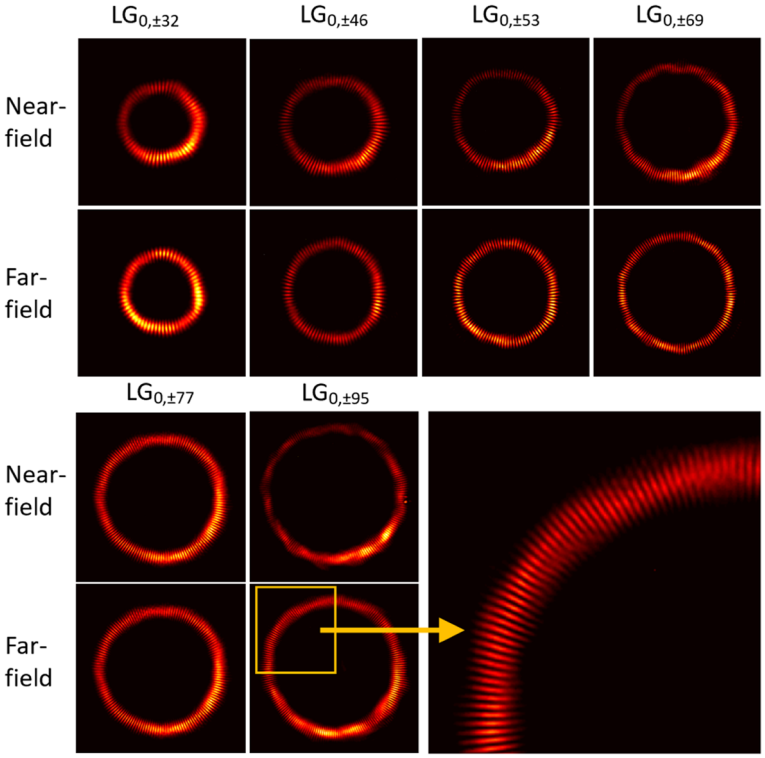

Fig. 6 Typical beam patterns obtained with different δ, when using lenses of focal length $f_1 = 150$ mm and $f_2 = 51.8$ mm. The lowest and highest order of eigenmodes obtained are $LG_{0,\pm 32}$ ($\delta = 4.5$ mm) and $LG_{0,\pm 95}$ ($\delta = 5.6$ mm) under the pump power of 1.20 W

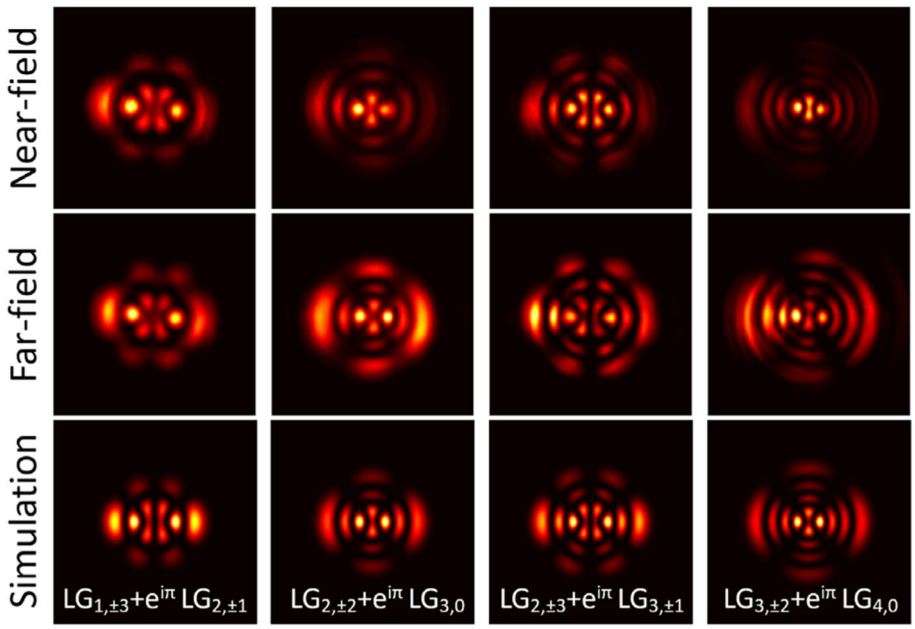

Fig. 7 Typical beam patterns obtained with different δ, when using lenses of $f_1 = 150$ mm and $f_2 = 25$ mm, under a pump power of 1.03 W

Table 1 The single LG mode operation achieved with different lenses (L2)

Focal length	Shape	Pump power	Radial indices *p*	Angular indices *m*	Range of δ	Output power range
15.3 mm	Plano-Convex	1.03 W	0	1–5	0.20–0.37 mm	10–57 mW
25.4 mm	Plano-Convex	1.03 W	0–4	2–16	0.70–1.23 mm	123–155 mW
33.9 mm	Plano-Convex	1.03 W	0	10–33	1.30–1.80 mm	18–191 mW
51.8 mm	Bi-Convex	1.03 W	0	27–75	4.42–5.14 mm	11–124 mW
		1.20 W	0	32–95	4.50–5.60 mm	2–132 mW

eigenmodes in the elliptical coordinate system), formed by two LG modes with intermodal phase π. We have numerically simulated a number of these modes and their spatial profiles are shown in the third row of Fig. 7. An experimental investigation into the origin of the symmetry-breaking within our cavity is ongoing.

The effect of even stronger SA was investigated with the use of a lens with an even shorter focal length of 15.3 mm. Here, single-mode outputs with $p = 0$ and $m = 1$–5 were recorded. Table 1 summarizes the ranges of LG modes which could be obtained with each lens used in the experiment. By using different lenses as L2 in the cavity, and by tuning the incident pump power, the lowest-order and highest-order modes which could be generated were $LG_{0,\pm1}$ and $LG_{0,\pm95}$ respectively. The slope efficiency of the laser was determined by SA-induced loss and spatial overlap efficiency between a gain volume and a laser mode, and it was measured to be 10–20%. Our theoretical analysis along with experimental results provide the optimization criteria for generating a desired single-LG mode output via the process of mode selection using intracavity spherical aberration.

Conclusion

In conclusion, we have analyzed and experimentally verified the influence of intracavity SA on the range of single-mode LG output that can be generated from a diode-end-pumped Nd:YVO_4 laser. We found that sufficient SA to distinguish neighboring modes of the laser cavity is necessary for single-transverse-mode operation of a desired LG mode. The strength of the SA must be carefully considered as it will also cause non-negligible defocusing loss to the oscillating LG mode since the mode itself has a finite width. By using lenses with shorter focal length to enhance the SA and resultant mode-selecting capability, LG modes with small angular indices m as low as ± 1 and non-zero radial indices p of up to 4 were obtained. By using a long focal length lens to reduce the SA-induced losses on high order modes, the highest angular index m reached ± 95. These results demonstrate the strong potential and relative ease by which LG modes with customizable mode characteristics can be generated directly from a simple, diode-end-pumped solid state laser system.

Abbreviations
LG: Laguerre-Gaussian; SA: Spherical Aberration.

Acknowledgements
The authors acknowledge the help from Dr. Andrew James Lee on both technical discussion and language editing.

Authors' contributions
Q. Sheng proposed the idea and designed the experiment. A. Wang, M. Wang, Z. Shi, and J. Liu finished the experiment. Y. Ma and S. Wang made the theoretical analysis and processed the data. W. Shi, J. Yao and T. Omatsu supervised the work. All authors read and approved the final manuscript.

Funding
National Natural Science Foundation of China (61975146 & 62075159); Major Scientific and Technological Innovation Projects of Key R&D Plans in Shandong Province (2019JZZY020206). Takashige Omatsu acknowledges support from KAKENHI Grants-in-Aid (Nos. JP18H03884) of the Japan Society for the Promotion of Science (JSPS) and the Core Research for Evolutional Science and Technology program (No. JPMJCR1903) of the Japan Science and Technology Agency (JST). Sijia Wang acknowledges support from Foundation for Distinguished Young Scholars of China Academy of Space Technology (2021).

Availability of data and materials
The data that support the findings of this study are available from the corresponding author on reasonable request.

Declarations

Ethics approval and consent to participate
Not applicable

Consent for publication
Not applicable

Competing interests
The authors declare that they have non-financial competing interests.

Author details
[1]School of Precision Instrument and Optoelectronics Engineering, Institute of Laser and Optoelectronics, Tianjin University, Tianjin 300072, China. [2]Key Laboratory of Optoelectronic Information Science and Technology (Ministry of Education), Tianjin University, Tianjin 300072, China. [3]Molecular Chirality Research Center, Chiba University, 1-33 Yayoi-cho, Inage-ku, Chiba 263-8522, Japan. [4]Qian Xuesen Laboratory of Space Technology, China Academy of Space Technology, Beijing 100094, China.

Received: 8 December 2021 Accepted: 4 February 2022
Published online: 10 February 2022

References

1. Forbes A. Structured light from lasers. Laser Photonics Rev. 2019;13(11):1900140.
2. Omatsu T, Miyamoto K, Lee AJ. Wavelength versatile optical vortex lasers. J Opt. 2017;19(12):123002.

3. Willner AE, Huang H, Yan Y, Ren Y, Ahmed N, Xie G, Bao C, Li L, Cao Y, Zhao Z, Wang J, Lavery MPJ, Tur M, Ramachandran S, Molisch AF, Ashrafi N, Ashrafi S. Optical communications using orbital angular momentum beams. Adv Opt Photon. 2015;7(1):66–106.
4. Forbes A, de Oliveira M, Dennis MR. Structured light. Nat Photonics. 2021;15:253–62.
5. Fu S, Zhai Y, Zhang J, Liu X, Song R, Zhou H, Gao C. Universal orbital angular momentum spectrum analyzer for beams. PhotoniX. 2020;1:19.
6. Tung JC, Hsieh YH, Omatsu T, Huang KF, Chen YF. Generating laser transverse modes analogous to quantum green's functions of two-dimensional harmonic oscillators. Photon Res. 2017;5(6):733–9.
7. Tung JC, Ma YY, Miyamoto K, Chen YF, Omatsu T. Bottle beam generation from a frequency-doubled Nd:YVO_4 laser. Sci Rep. 2018;8:16576.
8. Shen Y, Nape I, Yang X, Fu X, Gong M, Naidoo D, Forbes A. Creation and control of high-dimensional multi-partite classically entangled light. Light-Sci App. 2021;10(5):796–805.
9. Chen YF, Tung JC, Hsieh MX, Hsieh YH, Liang HC, Huang KF. Origin of continuous curves and dotted spots in laser transverse modes with geometric structures. Opt Lett. 2019;44(24):5989–92.
10. W. Koechner, Solid-state laser engineering, 6th ed. (Semantic Scholar 2006), pp.211–231. https://link.springer.com/book/10.1007%2F0-387-29338-8.
11. Song R, Gao C, Zhou H, Fu S. Resonantly pumped Er:YAG vector laser with selective polarization states at 1.6 μm. Opt Lett. 2020;45(16):4626–9.
12. Song R, Liu X, Fu S, Gao C. Simultaneous tailoring of longitudinal and transverse mode inside an Er:YAG laser. Chin Opt Lett. 2021;19(11):111404.
13. Ito A, Kozawa Y, Sato S. Generation of hollow scalar and vector beams using a spot-defect mirror. J Opt Soc Am A. 2010;27(9):2072–7.
14. Lee AJ, Omatsu T, Pask HM. Direct generation of a first-stokes vortex laser beam from a self-raman laser. Opt Express. 2013;21(10):12401–9.
15. Zhao Y, Liu Q, Zhou W, Shen D. ~1 mJ pulsed vortex laser at 1645 nm with well-defined helicity. Opt Express. 2016;24(14):15596–602.
16. Bisson J-F, Senatsky Y, Ueda K-I. Generation of Laguerre-Gaussian modes in Nd:YAG laser using diffractive optical pumping. Laser Phys Lett. 2005;2(7):327–33.
17. Ma Y, Lee AJ, Pask HM, Miyamoto K, Omatsu T. Direct generation of 1108 nm and 1173 nm Laguerre-Gaussian modes from a self-raman Nd:$GdVO_4$ laser. Opt Express. 2020;28(16):24095–103.
18. Yonezawa K, Kozawa Y, Sato S. Generation of a radially polarized laser beam by use of the birefringence of a c-cut Nd:YVO_4 crystal. Opt Lett. 2006;31(14):2151–3.
19. Ito A, Kozawa Y, Sato S. Selective oscillation of radially and azimuthally polarized laser beam induced by thermal birefringence and lensing. J Opt Soc Am B. 2009;26(4):708–12.
20. Chuang C-H, Ho C-Y, Hsiao Y-C, Chiu C-P, Wei M-D. Selection rule for cavity configurations to generate cylindrical vector beams with low beam quality factor. Opt Express. 2021;29(4):5043–54.
21. Chen YF, Lan YP. Dynamics of helical-wave emission in a fiber-coupled diode end-pumped solid-state laser. Appl Phys B. 2001;73(1):11–4.
22. Senatsky Y, Bisson J-F, Shelobolin A, Shirakawa A, Ueda K. Circular modes selection in Yb:YAG laser using an intracavity lens with spherical aberration. Laser Phys. 2009;19(5):911–8.
23. Senatsky Y, Bission JF, Li J, Shirakawa A, Thirugnanasambandam M, Ueda K. Laguerre-Gaussian modes selection in diode-pumped solid-state laser. Opt Rev. 2012;19(4):201–21.
24. Thirugnanasambandam MP, Senatsky Y. Generation of very-high order Laguerre-Gaussian modes in Yb:YAG ceramic laser. Laser Phys Lett. 2010;7(9):637–43.
25. Thirugnanasambandam MP, Senatsky Y, Senatsky A, Ueda K. Multi-ring modes generation in Yb:YAG ceramic laser. Opt Mater. 2011;33(5):675–8.
26. Wang M, Ma Y, Sheng Q, He X, Liu J, Shi W, Yao J, Omatsu T. Laguerre-Gaussian beam generation via enhanced intracavity spherical aberration. Opt Express. 2021;29(17):27783–90.
27. Sheng Q, Wang M, Ma H, Qi Y, Liu J, Xu D, Shi W, Yao J. Continuous-wave long-distributed-cavity laser using cat-eye retroreflectors. Opt Express. 2021;29(21):34269–77.
28. Phillips RL, Andrews LC. Spot size and divergence for Laguerre Gaussian beams of any order. Appl Opt. 1983;22(5):643–4.
29. Wang J, Yang J-Y, Fazal IM, Ahmed N, Yan Y, Huang H, Ren Y, Yue Y, Dolinar S, Tur M, Wilner AE. Terabit free-space data transmission employing orbital angular momentum multiplexing. Nat Photonics. 2012;6(7):488–96.
30. Woerdemann M, Alpmann C, Esseling M, Denz C. Advanced optical trapping by complex beam shaping. Laser Photonics Rev. 2013;7(6):839–54.

Publisher's Note